



Investigating the effects of printing temperatures and deposition on the compressive properties and density of 3D printed polyetheretherketone

Pedro Rendas¹ · Lígia Figueiredo² · Ricardo Cláudio^{3,4} · Catarina Vidal^{1,5} · Bruno Soares^{1,5}

Received: 27 July 2023 / Accepted: 17 November 2023
© The Author(s) 2023

Abstract

Polyetheretherketone (PEEK) is a biocompatible high-performance thermoplastic that can be processed through material extrusion (ME) additive manufacturing (AM) for load-bearing implant applications. In this work, density measurements and compression testing were used to investigate the relation between printing temperatures and deposition patterns of PEEK 3D printed samples. Different deposition patterns were tested with different nozzle and zone heater temperatures to observe how the heat input from the printing process influenced the deposition stability with different nozzle paths. Compression test results showed that samples with concentric-based deposition patterns resulted in higher compressive yield strength and modulus than the rectilinear samples. These results were correlated with the samples' void contents estimated from density measurements. Both the highest 0.2% offset yield strength of 100.3 MPa and the highest modulus of 3.58 GPa were obtained with an interlayer offset deposition which resulted in reductions in estimated void contents between 48 and 72% in relation to concentric deposition. Different printing temperatures and deposition sequences were tested, where higher printing temperatures resulted in lower yield strength and stiffness. Alternating deposition between the outer and inner lines of the concentric pattern resulted in a reduction of about 43% in void contents and increased elastic modulus and yield strength from 3.12 to 3.40 GPa and 94.4 to 95.2 MPa respectively. The results from this work suggest that the relation between printing temperatures and deposition strategy for different print geometries plays a significant role in the ME-AM of PEEK for high-performance applications.

Keywords Polyetheretherketone · PEEK · Material extrusion · Additive manufacturing · Mechanical properties

1 Introduction

Additive manufacturing (AM) has been one of the main subjects of recent research in the technology and engineering fields. With AM, complex three-dimensional (3D) geometries can be fabricated based on computer-aided design (CAD) virtual models by consecutively adding material until the final part is obtained. This makes AM flexible to design adjustments and can reduce product development costs [1] while its additive nature results in less material waste on manufacture [2]. Considering this, recent improvements in the reliability of AM technology and new material options have made it highly suitable for industries focused on the manufacture of customized products for demanding applications like the aerospace and biomedical industries [3].

In the biomedical field in particular AM, which is also commonly referred to as 3D printing, can display its full potential. In this field, AM's ability to produce complex

✉ Pedro Rendas
p.rendas@campus.fct.unl.pt

¹ UNIDEMI, Department of Mechanical and Industrial Engineering, NOVA School of Science and Technology, Universidade NOVA de Lisboa, 2829-516 Caparica, Portugal

² Bioceramed-Cerâmicos Para Aplicações Médicas S.A, São Julião do Tojal, 2660-360 Loures, Portugal

³ CDP2T, ESTSetúbal, Instituto Politécnico de Setúbal, Setúbal, Portugal

⁴ IDMEC, Instituto Superior Técnico, Lisbon, Portugal

⁵ Laboratório Associado de Sistemas Inteligentes, 4800-058 Guimarães, Portugal

3D structures can be used for scaffold production in tissue engineering, while its design flexibility combined with the use of biocompatible materials allows for the 3D printing of implantable medical devices tailored to the patient [4–6]. For these reasons, the use of biocompatible thermoplastic polymers has been researched for their processability through material extrusion (ME) AM techniques, also known as Fused Deposition Modelling ((FDM®, Stratasys, USA) or fused filament fabrication (FFF), both in their bulk state or as a composite's matrix. One example of this is the use of FFF for the fabrication of polypropylene–tricalcium phosphate (PP–TCP) scaffolds with controlled porosity to increase cell growth and adhesion [7].

Among biocompatible thermoplastics processable through ME, polyetheretherketone (PEEK) has been highlighted in research as the leading biomaterial candidate for the replacement of metals in load-bearing medical implant applications [8–10]. With the possibility of using AM, the viability of patient-specific designs increases expanding the range of potential applications for PEEK which include dental prosthetics, interbody fusion, arthroplasty and even bone repair or artificial bone replacement [11–13]. PEEK's potential is attributed to its higher mechanical performance, with specific strength and stiffness closer to that of human bone, and to its chemical stability which make it resistant to in vivo degradation [10]. In its potential for load-bearing implant manufacture, PEEK's mechanical performance plays an important role as its bone-like stiffness can help prevent stress shielding of the treated bone whereas the high stiffness of metallic implant materials hinders bone stimulation and has been shown to lead to bone resorption [14]. Despite this potential, there are still some issues to be solved regarding surface roughness, dimensional accuracy and mechanical behaviour of 3D printed components for high-performance applications [15]. Considering this, the relations between FFF's process variables and the mechanical behaviour of 3D printed PEEK are an important subject of research to address the requirements for medical device manufacture.

Printing parameters are strongly related to the mechanical behaviour of 3D printed PEEK and different approaches to process parametrization often result in different mechanical properties for printed components. Among printing parameters, build orientation can be one of the most impactful parameters since it affects how the loads are carried through the printed specimen [16]. This is related to the weak bonding interfaces formed between the deposited lines and layers, leading 3D printed components to exhibit an anisotropic behaviour. Loads carried axially through the deposited lines are transferred more efficiently than those causing shear in these weak bonding interfaces [16–19]. For this reason, build orientations where the deposited lines and layers are oriented parallel to the loads have resulted in PEEK samples with higher strength [20, 21]. In addition to this, the infill

percentage parameter determines the density of the print and is, therefore, related to the sample's effective cross-section for load support. PEEK samples printed with 100% infill and build orientation aligned with the loads resulted in ductile fracture after yield whereas brittle fracture initiating in the deposited material's bonding interfaces was observed for samples with build orientation perpendicular to the loads [22]. This suggests that build orientation and infill are some of the most important settings for stronger PEEK 3D prints.

Assuming fully dense prints with aligned build orientation, the improvement of 3D printed PEEK's mechanical performance through parameter adjustment can be challenging. Research suggests that the strength and stiffness of 3D printed PEEK can be increased through the improvement of interfacial bonding which can be achieved through the increase of contact areas between the deposited material and consequent reduction of void volume. The void contents of FFF prints are typical of the material's deposition and have been shown to represent as much as 8% of the volume of PEEK samples even for 100% infill prints [22]. These void contents affect the mechanical behaviour of PEEK 3D prints given its high notch sensitivity and crack propagation rates [23, 24] where crack initiation can be promoted by higher void contents. This is why PEEK samples with higher porosity percentages have displayed lower strength [22, 25]. Considering this, the various printing parameters and their interplays can have different effects on the void contents of 3D prints and previous works have suggested the use of negative line-to-line distance (overlapping lines) and interlayer line translation as effective approaches to reduce the void contents of FFF printed parts [26, 27]. Additionally, a recent work has shown that interlayer line translation can efficiently improve interlayer bonding and reduce the void contents of PEEK prints, resulting in higher tensile and flexural strength and stiffness [28].

Apart from the reduction of void presence, the interfacial adhesion of FFF prints can also be increased by promoting molecular diffusion to the bonding interfaces of the deposited material [29]. This occurs at the final stage of the bonding process typical of FFF following neck growth between the bonded material as described in previous works [30]. Here, printing temperatures play an important role as these parameters are directly related to the temperatures of the deposition zone and of the deposited material. Molecular diffusion to bonding interfaces can also be improved by post-printing annealing treatments with slower heating/cooling rates which result in increases in both strength and stiffness but can also promote brittle failure of 3D printed PEEK samples [28, 31]. These results can also be attributed to the increase of PEEK's crystalline phase which is promoted by the slower cooling rates of the annealing treatment and is related to higher strength and modulus of PEEK samples [32].

The effects of nozzle and ambient temperatures on the interfacial bonding of printed PEEK can be difficult to assess. Higher nozzle temperatures can increase molecular mobility and have been shown to improve the dynamic mechanical behaviour of PEEK prints [21] while higher printing ambient temperatures of up to 90°C increased interlayer bonding together with the tensile and flexural strength of PEEK samples [33]. Although these temperatures can affect bonding conditions as previously mentioned, the temperature difference between the deposited material and the deposition zone is also significantly dependent on the deposition path [34]. Furthermore, nozzle temperature is also related to the deposited material's viscosity which can lead to instability in the extrusion flow. This instability can result in irregular deposition and lead to the appearance of larger scale void defects [28]. All of this suggests that printing temperatures have a significant influence not only on the molecular bonding of PEEK prints but also on the behaviour of the material upon deposition and the overall structural integrity of the 3D printed component.

PEEK's 3D printing for high-performance applications is still a challenge to researchers since the presence of void defects and differences in the bonding upon deposition result in PEEK 3D prints with strength and stiffness lower than their injection moulded counterparts [20]. To take advantage of PEEK's 3D printing design flexibility in face of an application's mechanical requirements, a deeper understanding of the effects of relevant FFF parameters for different sample configurations is required. For this reason, there is the need to address the effects of FFF parameters focusing specifically on deposition stability and bonding quality and their effects on void content reduction.

In this work, the effects of printing temperatures on compressive properties and in the presence of void defects in PEEK prints are studied for different deposition strategies. Although the influence of FFF parameters such as line dimension, nozzle temperature and printing speed on the compressive properties of printed PEEK has been described in previous works [35], research has disregarded the effects of the deposition strategy and its relation to temperature parameters for 3D printed PEEK. The aim of this work is to document the effects of nozzle and deposition zone preheating temperatures on PEEK compressive specimens printed with different deposition strategies where deposition stability and bonding quality can vary significantly. For this, the relations between printing temperatures and the deposition pattern and sequence are studied through the compressive properties and density of 3D printed PEEK.

2 Materials and methods

2.1 Materials and equipment

The samples for the experiments were printed using neat PEEK filament (Apium PEEK 450 Natural, Apium Additive Technologies GmbH, Karlsruhe, Germany) with a diameter of 1.75 mm. Filament specifications detail the material properties as 1.3 g/cm³ for filament density, glass transition temperature of 143°C, a melting temperature of 342°C and elastic modulus and tensile strength of 4 GPa and 98 MPa, respectively [36]. The PEEK filament was dried before printing the samples in the Apium F300 filament dryer (Apium Additive Technologies GmbH, Karlsruhe, Germany) for 4 h at 120 °C and then maintained at 60 °C for conditioning and printing.

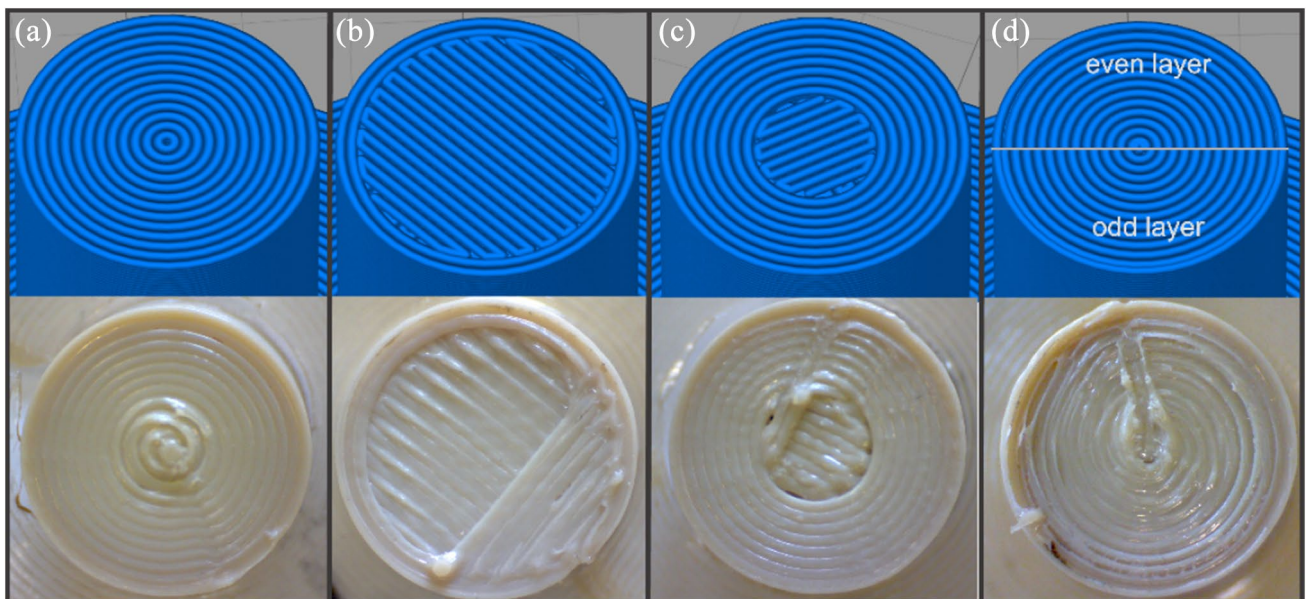
In this work, the samples were printed using Apium's P220 printer (Apium Additive Technologies GmbH, Karlsruhe, Germany). This printer is designed for high-performance printing of high-temperature materials such as PEEK and includes some features that help improve the quality of PEEK printed samples. Some of these features are an extruder liquid-cooling system which has been shown to improve filament feeding and improve flow stability [37] and an adaptive heating system around the nozzle, henceforth referred to as zone heater, that distributes heat to the deposition area around the nozzle and improves layer adhesion and dimensional accuracy by heating and controlling cooling rates of the uppermost layers. Deposition zone preheating is essential to obtain good quality PEEK prints and has been demonstrated to increase the crystallinity and improve the mechanical properties of 3D printed PEEK samples [38]. With these materials and equipment, high-quality samples were obtained using different printing parameters.

2.2 Experimental design

To investigate the effects of printing temperatures and deposition on the density and compressive properties of PEEK samples, compressive specimens were printed and tested with different nozzle temperatures (NT) and zone heater temperatures (ZHT). These temperatures were varied according to Table 1 from the standard print settings provided by the manufacturer of 485 °C for NT and 130 °C for ZHT which were set as the "01" temperature combination. For this, the NT and ZHT were varied to test different degrees of heat input for the printing process which also include lower NT combined with higher ZHT for "05" referenced samples and a much higher ZHT of 170 °C for "06" samples.

Table 1 Experimental design for NT, ZHT and deposition configurations for tested samples

Temperature reference	NT [°C]	ZHT [°C]	Deposition pattern	Label
01	485	130	Concentric	01C
			Rectilinear	01X
			Outer concentric—inner rectilinear	01 M
			Interlayer offset concentric	01S
02	485	150	Concentric	02C
			Rectilinear	02X
			Outer concentric—inner rectilinear	02 M
			Interlayer offset concentric	02S
03	495	130	Concentric	03C
			Rectilinear	03X
			Outer concentric—inner rectilinear	03 M
			Interlayer offset concentric	03S
04	495	150	Concentric	04C
			Rectilinear	04X
			Outer concentric—inner rectilinear	04 M
			Interlayer offset concentric	04S
05	475	150	Concentric	05C
			Rectilinear	05X
			Outer concentric—inner rectilinear	05 M
			Interlayer offset concentric	05S
06	485	170	Concentric	06C
			Rectilinear	06X
			Outer concentric—inner rectilinear	06 M
			Interlayer offset concentric	06S

**Fig. 1** Deposition patterns and printing results for configurations “C” (a), “X” (b), “M” (c) and “S” (d)

Each of these temperature settings was then used for 4 different deposition strategies as represented in Fig. 1. Two of these strategies included a concentric infill for samples labelled with “C” (Fig. 1a) and an alternating angle ($-45^{\circ}/45^{\circ}$) rectilinear infill for samples labelled with “X” (Fig. 1b). The configuration labelled as “M” (Fig. 1c) corresponds to a concentric deposition where the 5 innermost concentric laps were replaced with an alternating rectilinear infill to solve extrusion issues with small radius concentric deposition. Lastly, label “S” (Fig. 1d) corresponds to a concentric infill with an interlayer offset, as presented in previous works [28]. For each of the sample configurations, a label was attributed combining temperature setting configuration with deposition strategy as displayed in the rightmost column of Table 1.

In addition to this, this experimental work also addressed the printing process's heat input for different deposition sequences given the importance of the nozzle as a heat source. For this, the concentric infill sample “C” for the highest strength temperature setting was also printed with different deposition sequences for the concentric laps. Slicer software normally generates concentric deposition either starting from the inside or from the outside with the sequence remaining the same throughout the print. In this work, different concentric deposition sequences were also tested, including a strategy where deposition alternates between outer laps and inner laps which corresponds to the suffix “A”, and the strategy where deposition switches back and forth from outside-to-inside to inside-to-outside between each layer which corresponds to the suffix “I”. This resulted in two new printing configurations referenced as 01C-A and 01C-I which are schematically illustrated in Fig. 13. Samples of these configurations were printed and submitted to density measurements and compression testing for comparison with sample 01C to assess the effects of different deposition sequences.

2.3 Samples' 3D printing and testing

The G-code printing files were generated using the slicer software Simplify3D (v4.1.2). All samples were printed using a nozzle of 0.4 mm of diameter and with the same settings for the line dimensions, meaning that line width is equivalent to the nozzle diameter and layer height is 0.2 mm. Printing speed was set to 1200 mm/min with an outline underspeed factor of 50%. Also, specimens were all printed with the print bed temperature set for 130 °C and a large single layer brim with about 10 mm of width was included to help with bed adhesion and prevent the detachment of the print. With these parameters, the printing files were generated for a vertical build orientation with the “C”, “X” and “M” deposition strategies described in the previous section for the circular layers. The interlayer line offset samples “S”

G-code files were obtained using a python script that uses the file generated for samples “C” and rewrites the offset toolpath for the even numbered layers.

Considering the different deposition samples, printing conditions can vary significantly with both printing temperatures and deposition. These conditions are thus related to effective line width determined by spreading upon deposition [39] and to deposition stability as a consequence of pressure variations in the filament feeding system [40, 41]. Extrusion consistency is especially important for deposition strategies that present different line lengths as it is the case for the concentric pattern. Concerning this, the printer's extrusion was calibrated iteratively until the concentric and rectilinear depositions presented dense layers with little evidence of void defects. In addition to this, the G-code files of the concentric samples were edited using another python script that applies a factor to “E” movements' length based on the full lap's length. After some testing, different factors between 0.8 and 0.95 were applied to 6 of the innermost laps for both “C” and “S” samples. However, it is important to note that the values used in this adjustment may depend on test specimen size and geometry. Results from this calibration can be seen in Fig. 2 where the influence of extrusion calibration in the void contents and overall quality of PEEK prints is evident. The end-result for the printed samples' deposition is provided in Fig. 1 for each of the configurations.

With the extrusion duly calibrated, compression test specimens were printed for the 6 temperature settings combined with the 4 deposition strategies, resulting in 24 print configurations. For each print configuration, a set of 5 samples were printed and tested. In addition to this, testing of the effects of deposition sequence on the concentric printed specimens added 2 different configurations, considering the reference temperatures. Following ASTM D695-96 guidelines, 5 cylindrical compression test specimens with 12.7 mm of diameter and double of that in length (25.4 mm) were printed for all 26 print configurations for a total of 130 test samples. Compression testing between plates was then performed for all samples at the standard test speed of 1.3 mm/min. These tests were conducted using a universal testing machine (INSTRON 1342, Instron Corp, Massachusetts, USA) equipped with a 250kN load cell from which the modulus of elasticity and the offset yield strength at 0.2% strain were calculated, all according to ASTM D695-96.

In addition to compression testing, density measurements were performed on all samples to obtain an estimate for void volume, as well as a quality control procedure to discard outlier samples. The density of the samples was measured according to the immersion method detailed in ISO 1183-1-2012 where the relation between the samples' weight and its weight immersed in a fluid, in this case distilled water, is used to calculate the samples' density. Although this standard refers to the density of void-free plastic, it can be used

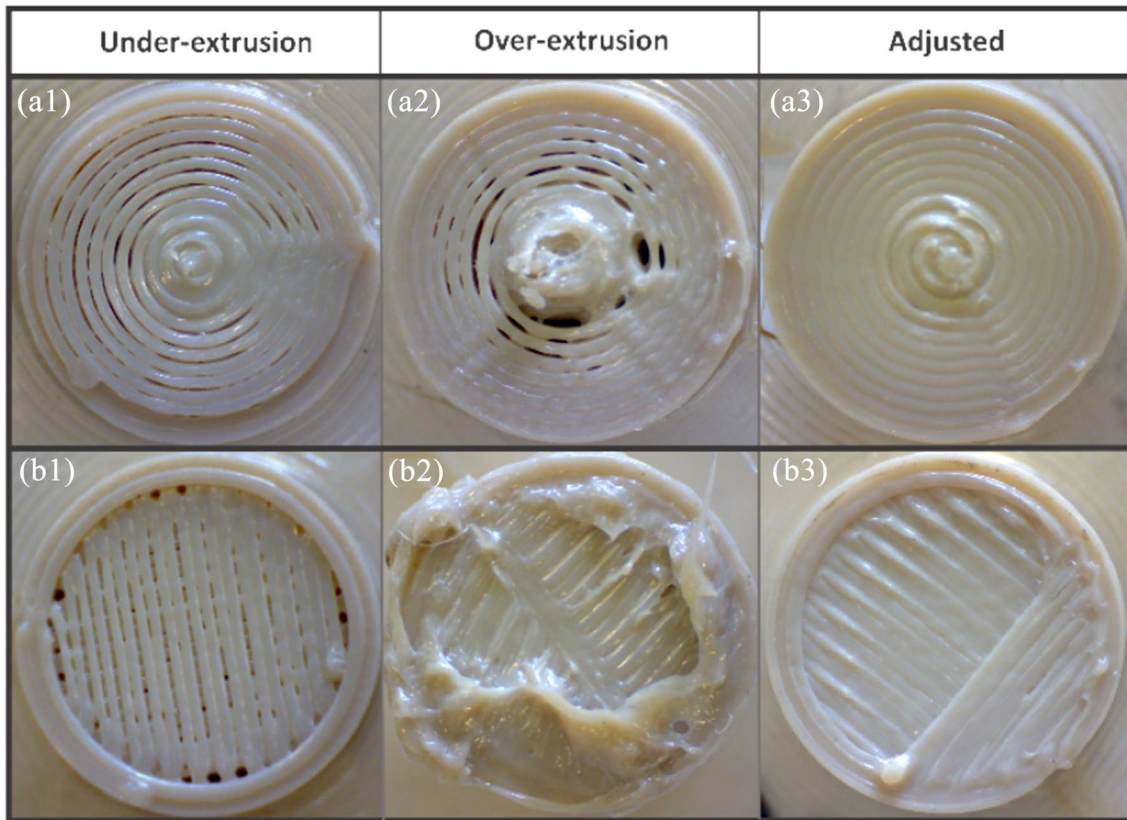


Fig. 2 Extrusion calibration in concentric samples 01C (a) and rectilinear samples 01X (b) with the radial cross-section of specimens with under-extrusion (a1, b1), with over-extrusion (a2, b2) and after extrusion adjustment (a3, b3)

to estimate the void contents of samples as the volume fraction of air based on the measured density of the samples. For this, the documented filament density of 1.3 g/cm^3 [36] was considered as the specific mass of the bulk PEEK. This estimation also assumes that there are no open porosities that would allow the fluid to infiltrate the samples. Considering this, density measurements were taken for all printed samples and the average density and corresponding void percentage was documented for each one of the configurations.

With this, the compressive properties and densities of the PEEK 3D printed samples were used to investigate the effects of printing temperatures for different deposition strategies. Furthermore, with the extrusion calibration performed in this work differences in print conditions were reflected in both the density and compression testing results thus allowing to investigate the effects of NT and ZHT on the deposition stability of 3D printed PEEK samples.

2.4 Calorimetry

Differential scanning calorimetry (DSC) tests were carried out to test the impact of the thermal processing from different deposition sequences in the transition temperatures and

crystallinity for configurations 01C, 01C-A and 01C-I. For this, samples were taken at half radius from the middle layers of compression test specimens. Testing was performed using a NETZSCH DSC 204 F1 Phoenix calorimeter (Erich NETZSCH GmbH & Co. Holding KG, Selb, Germany) and the thermal analysis was performed using the NETZSCH Proteus software. DSC testing was conducted at heating/cooling rates of $10 \text{ }^\circ\text{C/min}$ and with maximum temperature of $400 \text{ }^\circ\text{C}$ for 5 min. The glass transition (T_g) and melt temperatures (T_m) were obtained from the heating curve while the “hot” crystallization temperature (T_{hc}) was obtained from the cooling curve.

To determine the samples’ crystallinity, the ratio between the heat required to melt the sample and the theoretical heat of fusion of fully crystalline PEEK was calculated following the same method used in other works [32, 42, 43]. With this, the percentage of the crystalline phase was determined by the equation:

$$X_c(\%) = \frac{\Delta H_{endo} - \Delta H_{exo}}{\Delta H_c}, \quad (1)$$

where ΔH_{endo} is the melt enthalpy measured as the area under the melting endothermic peaks, ΔH_{exo} is the “cold” crystallization enthalpy measured as the area above the exothermic peaks of the heating curve and ΔH_c is the theoretical melt enthalpy of fully crystalline PEEK. Following the crystallinity percentage determination methods used by other authors, this theoretical melt enthalpy of fully crystalline PEEK corresponds to 130J.g^{-1} [44].

Table 2 Density and compression test results for different deposition patterns

	Density (g/cm ³)	Porosity (%)	Modulus, E (GPa)	Yield strength, $\sigma_{0.2\%}$ (MPa)
01X	1.236 ± 0.011	4.9 ± 0.27	2.95 ± 0.1	90.3 ± 1.8
01 M	1.265 ± 0.004	3.45 ± 0.20	3.23 ± 0.11	93.0 ± 2.5
01C	1.255 ± 0.010	2.68 ± 0.22	3.12 ± 0.06	94.4 ± 1.7
01S	1.285 ± 0.010	1.17 ± 0.10	3.44 ± 0.11	100.3 ± 1.2

3 Results and discussion

3.1 Deposition pattern

The results from the density measurements together with the compressive modulus and 0.2% offset yield strength for the baseline NT and ZHT specimens are provided in Table 2. In these results, the different deposition patterns produced samples with clear differences in void volume percentage. The estimated void volume calculated from density measurements revealed that the concentric pattern produces denser samples than the alternating angle rectilinear patterns as 01C samples presents an average estimated void volume of almost half of that of 01X samples.

The difference in void contents of these samples is also evident in macrographs of their respective longitudinal cross-sections (Fig. 3). In the concentric deposition (Fig. 3a), lines are placed vertically in consecutive layers which results in an equivalent concentric distribution of voids while in the rectilinear deposition voids are placed in a grid where the line interfaces from consecutive layers intercept. Considering this, the higher void contents of the rectilinear deposition can be attributed to two main factors:

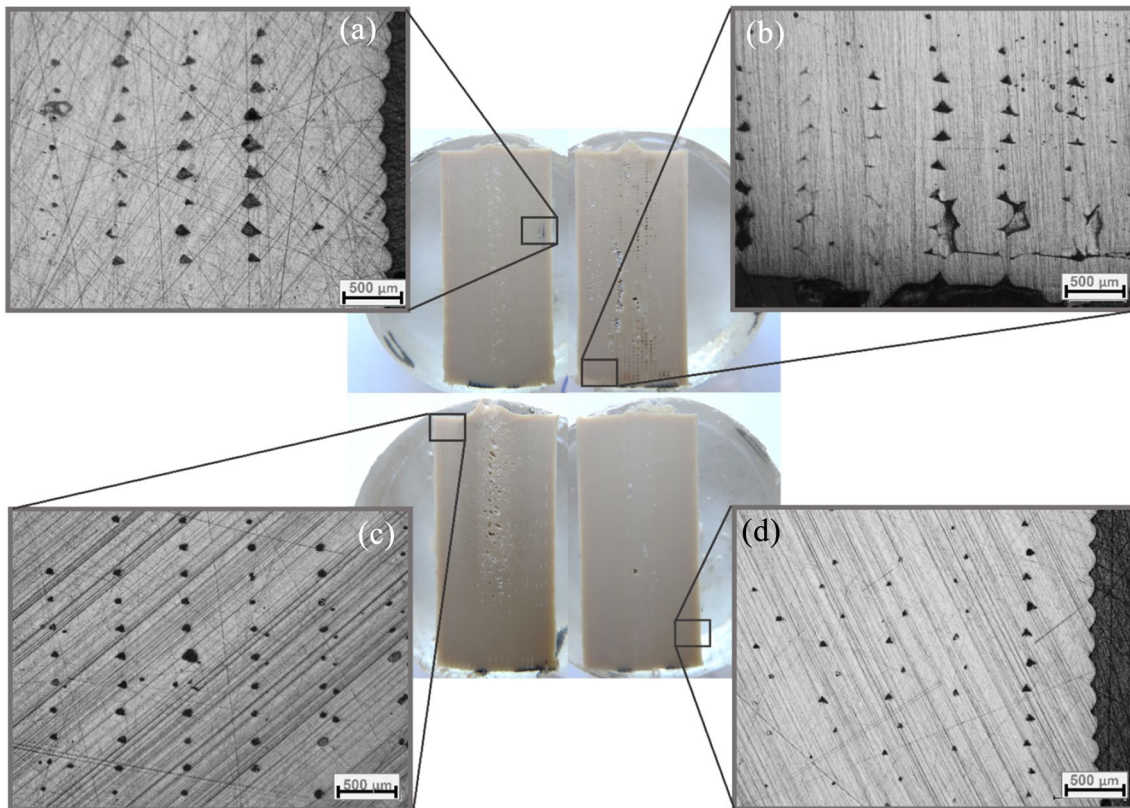


Fig. 3 Photographs and optic microscope macrographs of samples 01C (a), 01X (b), 01 M (c) and 01S (d) longitudinal cross sections taken through the samples' axis

the variations in line spreading as deposition crosses over the lines from the previous layer, and to gaps created in the perimeter-infill transition which were described in early works on FFF [45]. Also, due to overlap between infill and perimeter lines, the longer lines of the rectilinear deposition usually result in less spreading at mid length. This makes the void defects for the rectilinear deposition larger near the sample's centre as shown in Fig. 3b.

Concerning the remaining sample configurations, some positive effects can be reported for these deposition strategies. By limiting the rectilinear deposition to the innermost layers for samples 01 M, extrusion adjustments to the inner laps of concentric deposition can be avoided and the density of the samples can be easily improved in relation to the "X" deposition. However, evidence of void presence can still be seen in the transition from the concentric to rectilinear patterns in both Figs. 1c and 3c for the 01 M sample. Considering this, the hybrid configuration "M", although easier to implement, can be a less viable option for void reduction than extrusion adjustment in the concentric deposition. Lastly, the interlayer offset of samples 01S resulted in a significant increase of density with the estimated void volume being reduced about 56% compared to sample 01C. For this sample, the cross-section macrographs of Fig. 3d show less presence of void defects and their average size seems smaller compared to the other samples. These results are comparable to those obtained with micro-CT analysis reported in previous works [28] and further support the use of this offset in line placement for void content reduction.

Apart from this, the coloured photographs of the different deposition's cross-sections displayed in Fig. 3 reveal a fundamental issue with the extrusion for fully dense prints. With all configurations, there is a tendency for the formation of larger scale void defects near the axis of the cylindrical specimens. Since these specimens were built vertically, the area for each layer is relatively small which reduces the time

for the deposition zone to cooldown before the next layer begins. This results in temperature build-ups in the centre of the deposition zone where the deposited material remains in the molten state until the next layer starts. Consequently, the nozzle starts to stir the material that is still in the melt state and creates these large-scale void defects which can be seen in the samples cross-sections (Fig. 3) thus suggesting that excessive heat input can be very detrimental to deposition quality.

Compression test results for the different deposition patterns seem to be related to density measurements since both compressive yield strength and modulus increase for the patterns with lower estimated void volume. This relation can be observed in previous works documenting the compressive properties and density of 3D printed PEEK [35]. Nevertheless, the results from the present experiments display comparatively higher values for both strength and stiffness despite the lower densities measured, which can indicate that the procedure for extrusion calibration performed in this work is essential to produce high-quality PEEK prints.

For the different depositions, the lowest yield strength of 90.3 MPa and modulus of 2.95 GPa were obtained with the rectilinear pattern as expected. This is justified by the lower density of samples 01X which result in smaller effective cross-section areas for compressive load support. Conversely, the highest strength and modulus were obtained by the concentric deposition patterns where sample 01S averaged a compressive yield strength of 100.3 MPa and modulus of 3.44 GPa. Interestingly, the second highest compressive modulus was obtained for 01 M samples despite averaging a lower density. The reason for this can be more difficult to assess since it can be related to the suitability of process temperatures and other parameters for these depositions.

In addition to compression test results presented in Table 2, which are determined from the linear elastic

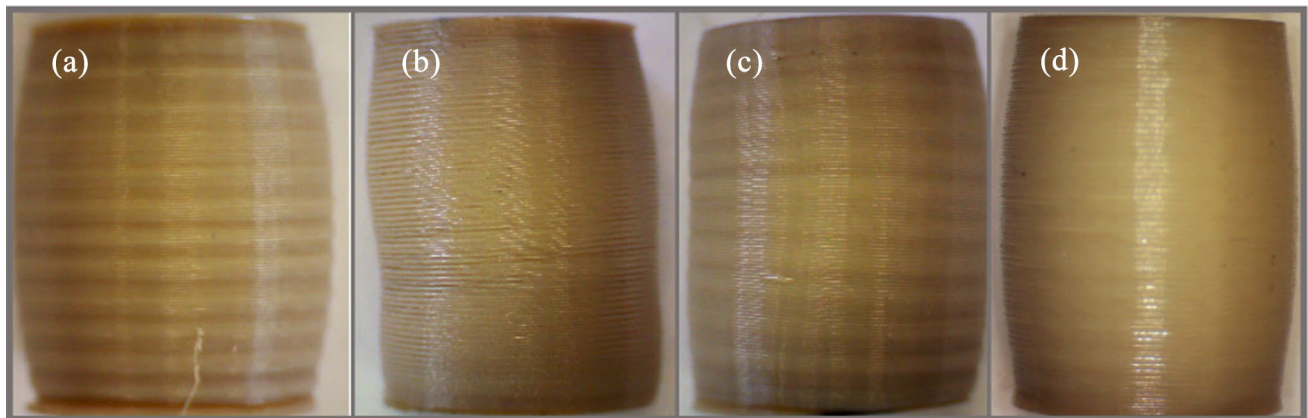


Fig. 4 Deformation of samples 01C (a), 01X (b), 01 M (c) and 01S (d)

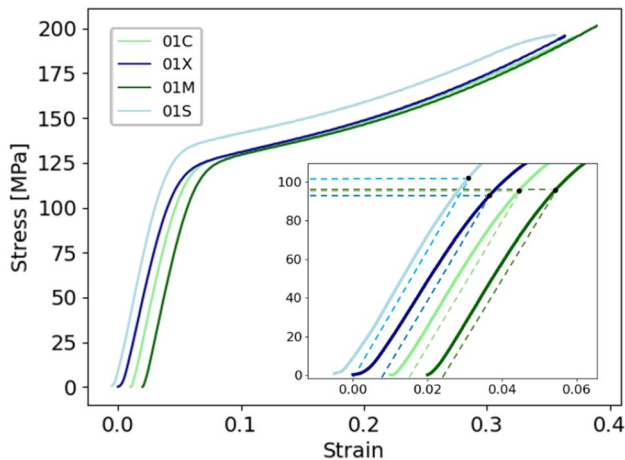


Fig. 5 Engineering stress–strain curves from the compression testing of the highest 0.2% offset yield strength “01” samples plotted with offsets of 1% in strain for visualization

behaviour. Figure 4 shows images of the deformed compressed specimens that were taken to examine plastic deformation. Also, Fig. 5 plots the stress–strain curves from the highest yield strength sample of each configuration with an offset of 1% in strain applied to the curves for better visualization.

The images of the deformed samples show typical barreling deformation for the concentric samples while the samples which included rectilinear deposition show unstable compression almost leading to buckling. This can suggest an uneven distribution of voids for samples 01X and 01 M. In any case, as compression loading in these configurations leads to pore compression, the plot of Fig. 5 shows that all samples tend for the same plastic behaviour after yield apart from sample 01S which shows a much higher yield strength despite its similar elastic modulus. Once again, this could be related to the reduced void contents of interlayer line offset deposition and further supports the use of such deposition strategies to increase the mechanical performance of 3D printed PEEK samples.

3.2 Nozzle and deposition zone preheating temperatures

The results for the baseline “01” temperature combination show that the tested deposition strategies produce samples with notable differences in both density and compressive properties. Different nozzle paths have different effects on extrusion stability since deposition pattern is related to both line length and heat input from the nozzle. Considering this, process temperatures like NT and ZHT can have different effects on material bonding and deposition behaviour depending on the layer pattern. This means that parametrization of printing temperatures should be performed according

to the deposition strategy and, to observe this, NT and ZHT temperatures were varied for the different samples.

The tested temperature combinations outlined in Table 1 are related to different heat inputs for the printing process. For configuration “02” the increase of ZHT is tested while “03” tests the increase of NT. Temperature combination “04” increases both NT and ZHT while “06” corresponds to a twofold increase in ZHT. Both these combinations represent the highest heat inputs tested for the printing process. Lastly, “05” prints correspond to a low NT, high ZHT configuration. With these combinations, it is possible to distinctively evaluate the effect of these process temperatures in the samples’ compressive properties and densities. The results from both density measurements and the compression testing of all samples are provided in Table 3 while results for each one of the tested deposition patterns were analysed separately.

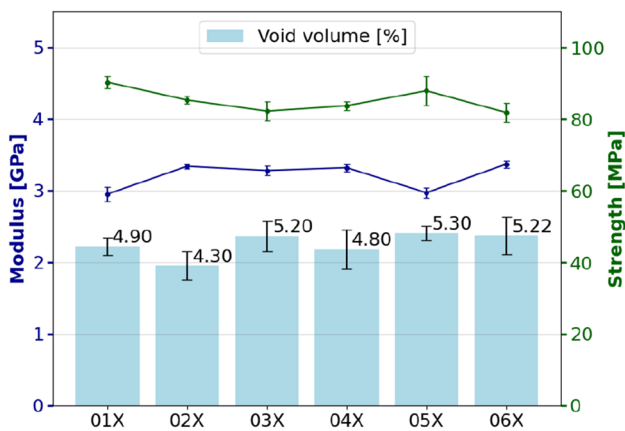
Between the tested deposition patterns, the results provided in Table 3 show that the compressive behaviour of 3D printed PEEK is closely related to the estimated void volume of the tested specimens. This relation between the compressive properties of printed PEEK and respective void contents can be seen in the results of previous works for both 100% infill PEEK specimens [35] and 3D printed macroporous PEEK scaffolds [46]. Higher void volume corresponds to smaller cross-section areas for compression load support thus resulting in lower compressive strength and stiffness.

Regarding the rectilinear deposition for samples “X”, the results shown in Fig. 6 suggest that increasing process temperatures, either through the nozzle or through deposition zone preheating, can increase the modulus of the samples. Both samples 02X and 03X displayed higher elastic modulus than samples 01X. However, samples 02X resulted in lower void percentage and higher yield strength than 03X. This suggests that increases in the temperature of the deposition zone can improve extrusion quality and consequently increase the samples’ stiffness. This can also be seen for samples 06X printed with ZHT of 170 °C which resulted in the highest compressive modulus of 3.37 GPa despite their lower density. Interestingly, the samples’ yield strength seems to vary inversely to compressive modulus despite the different void contents. Sample 01X which presented the lowest modulus of 2.95 GPa also resulted in the highest yield strength of 90.3 MPa closely followed by sample 05X which presents a higher estimated void volume.

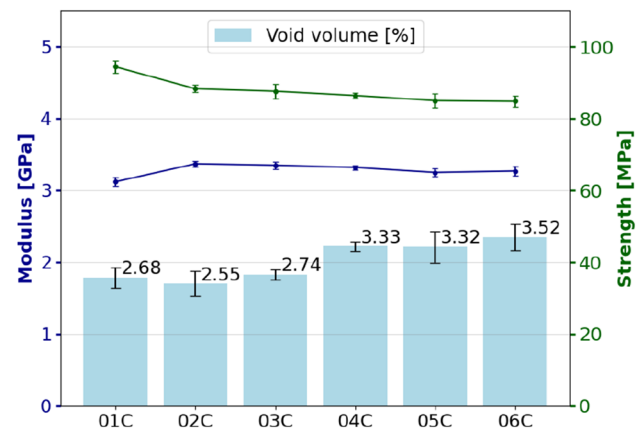
In the case of the concentric pattern, the results plotted in Fig. 7 suggest that the tested temperatures play a different role to that suggested for the rectilinear deposition. While, similarly, the highest strength of 94.4 MPa is presented together with the lowest modulus of 3.12 GPa in samples 01C, the highest modulus of 3.37 GPa in the concentric pattern also presents the second highest strength which corresponds to sample 02C. This can suggest that increases in

Table 3 Density measurements and compression test results for samples printed with different temperatures

	Density (g/cm ³)	Porosity (%)	Modulus, E_c (GPa)	Strength, $\sigma_{0.2\%}$ (MPa)
01X	1.236 ± 0.011	4.90 ± 0.27	2.95 ± 0.1	90.3 ± 1.8
01C	1.265 ± 0.004	3.45 ± 0.20	3.23 ± 0.11	93.0 ± 2.5
01 M	1.255 ± 0.010	2.68 ± 0.22	3.12 ± 0.06	94.4 ± 1.7
01S	1.285 ± 0.010	1.17 ± 0.10	3.44 ± 0.11	100.3 ± 1.2
02X	1.244 ± 0.010	4.30 ± 0.44	3.34 ± 0.03	85.3 ± 1.0
02C	1.267 ± 0.006	2.55 ± 0.26	3.37 ± 0.04	88.3 ± 1.0
02 M	1.253 ± 0.012	3.65 ± 0.16	3.33 ± 0.03	90.6 ± 1.1
02S	1.291 ± 0.003	0.72 ± 0.06	3.54 ± 0.06	97.3 ± 0.6
03X	1.232 ± 0.016	5.20 ± 0.46	3.28 ± 0.07	82.2 ± 2.7
03C	1.264 ± 0.006	2.74 ± 0.11	3.35 ± 0.05	87.6 ± 2.0
03 M	1.247 ± 0.013	4.04 ± 0.24	3.23 ± 0.13	86.1 ± 1.4
03S	1.289 ± 0.017	0.82 ± 0.15	3.58 ± 0.04	93.8 ± 2.0
04X	1.231 ± 0.025	5.30 ± 0.22	2.97 ± 0.07	87.9 ± 4.2
04C	1.257 ± 0.006	3.32 ± 0.33	3.25 ± 0.06	85.0 ± 1.9
04 M	1.239 ± 0.006	4.73 ± 0.20	3.13 ± 0.13	86.0 ± 2.3
04S	1.283 ± 0.024	1.29 ± 0.13	3.30 ± 0.02	95.6 ± 2.1
05X	1.238 ± 0.006	4.80 ± 0.60	3.32 ± 0.05	83.7 ± 1.3
05C	1.257 ± 0.013	3.33 ± 0.10	3.32 ± 0.03	86.4 ± 0.7
05 M	–	–	–	–
05S	1.285 ± 0.019	1.18 ± 0.13	3.58 ± 0.02	95.7 ± 0.9
06X	1.232 ± 0.017	5.22 ± 0.57	3.37 ± 0.05	81.8 ± 2.7
06C	1.254 ± 0.012	3.52 ± 0.28	3.27 ± 0.07	84.8 ± 1.5
06 M	–	–	–	–
06S	1.285 ± 0.014	1.12 ± 0.17	3.58 ± 0.02	92.8 ± 1.0

**Fig. 6** Density and compression test results plot for the “X” deposition

ZHT can improve stiffness without significant consequences to yield strength. However, this might not be the case for higher increases in temperature since samples 06C that were printed with a twofold increase in ZHT resulted in the highest void percentage, lowest yield strength and lower modulus. This is also reflected in the samples’ deformation where the barrelling observed in samples 01C transitions to slightly uneven compression for samples 04C which were printed

**Fig. 7** Density and compression test results plot for the “C” deposition

with higher temperatures (Fig. 8). For the concentric deposition, the lower heat input settings seem to improve the deposition quality as reflected in the lower void volume obtained for samples 01C, 02C and 03C but lowering this input any further can also reduce material spreading and increase the void contents as demonstrated in the results for sample 05C.

This relation between printing temperatures and deposition stability can also be observed in the results for samples

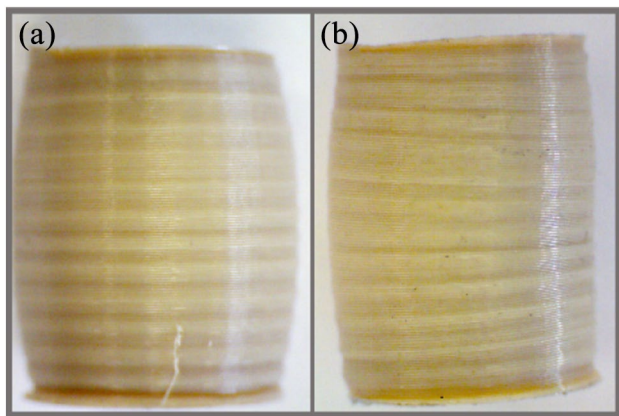


Fig. 8 Compression stability deformation comparison between samples 01C (a) and 04C (b)

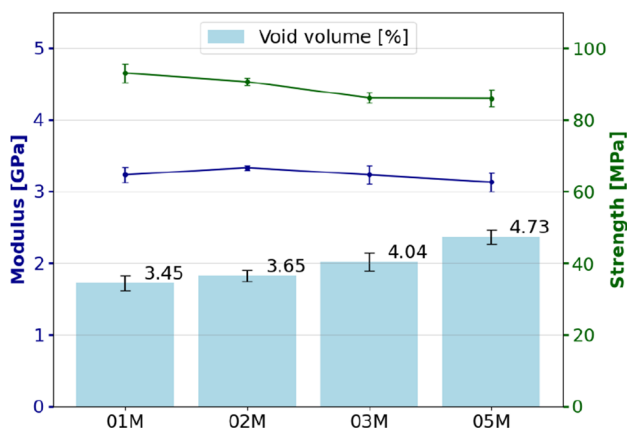


Fig. 9 Density and compression test results plot for the “M” deposition

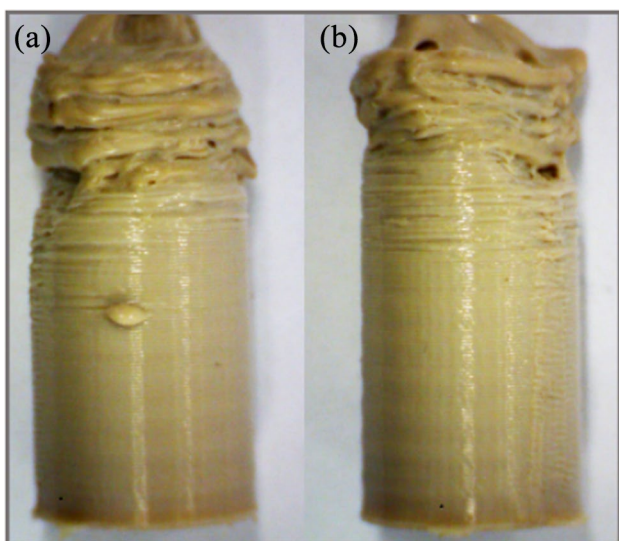


Fig. 10 Failed prints 05 M (a) and 06 M (b) due to insufficient cooling

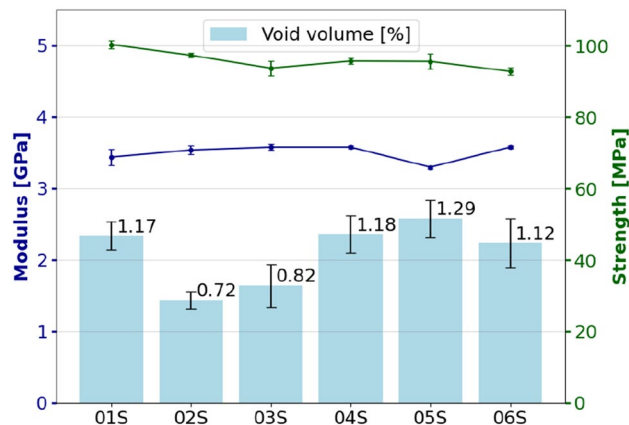


Fig. 11 Density and compression test results plot for the “S” deposition

with the “M” pattern (Fig. 9). In this configuration, excessive heat input in the printing process leads to temperature build-ups in the core of samples 04 M and 06 M destabilizing deposition and ultimately resulting in failed prints (Fig. 10). In these prints, the extruded material does not have enough time to solidify between layers and the rectilinear movements begin to stir the deposition zone which is still in its molten state. This issue is present in all the concentric based patterns “C”, “M” and “S” since the nozzle spends a considerable amount of layer printing time in the small inner region of the specimens. For “M” samples, this issue becomes critical due to overlapping extrusion in the rectilinear to concentric deposition interface. Considering this, only increases in ZHT seem to improve stiffness as seen for samples 02 M which displayed a slightly higher modulus of 3.33 GPa while the baseline temperatures used in sample 01 M resulted in the lowest estimated void volume and highest yield strength of 93.0 MPa.

Lastly, the “S” deposition results shown in Fig. 11 indicate that interlayer line offset not only reduces the void volume but can also increase deposition stability for higher printing temperatures. In these samples, the highest compressive modulus of 3.58 GPa is shared by 03S, 04S and 06S which correspond to the temperature settings with the highest heat input. Conversely, the highest void volume and lowest modulus of 3.3 GPa were obtained with 05S samples suggesting that NT can have significant effects on extrusion quality for this deposition. Furthermore, the highest yield strengths correspond to either the baseline temperature values with 100.3 MPa for samples 01S or to increased ZHT with 97.3 MPa for 02S. According to these results, slight increases in either ZHT or NT produced the samples with the lowest void volumes and increased stiffness. In this deposition, the increased temperatures can reduce viscosity and increase material spreading upon deposition as described in previous works [25, 47] which has the ability to improve the

interline gap filling effect of the line offset and thus results in lowest void volume samples with just 0.72% of void volume estimated for samples 02S.

Considering all this, the experimental results presented in this section show that the NT and ZHT can have different effects on print quality depending on the deposition strategy used for PEEK 3D printing. These effects seem to vary depending on the temperature profiles created in the deposition zone by nozzle path. Overall, deposition stability seems to decrease with variations to baseline NT while increases in ZHT with configuration “02” resulted in the samples with the lowest estimated void volume for all patterns with the exception of “M” which was obtained with 01M.

Concerning the compressive properties of the samples, the compressive modulus of the rectilinear samples appears to increase at the expense of yield strength where higher stiffness often resulted in samples with lower offset yield strength. As for the concentric-based patterns, excessive heat input seems to create temperature build-ups in the centre of the deposition region. With this, solidification is delayed which worsens deposition quality and increases void contents on the prints thus resulting in lower compressive yield strength and modulus. However, this is not the case for the interlayer line offset pattern “S” where increases in printing temperatures can lead to better gap fill and higher modulus.

Of all the tested configurations, “S” deposition presents the best results with the lowest estimated void volume of 0.72% for 02S, highest yield strength of 100.3 MPa for 01S and the highest modulus of 3.58 GPa shared between 03S, 04S and 06S. These values for compressive modulus are comparable to the modulus of 3.51 GPa presented in previous works for 3D printed 5% carbon fibre reinforced PEEK (CFR-PEEK) [48] that supported the use of these 3D printed PEEK for high-performance implant applications with mechanical property requirements (Fig. 11).

3.3 Deposition sequence

The different effects of printing temperatures in the tested deposition patterns outlined in the previous section show that heat input from the nozzle or from the zone heater plays an important role in the 3D printing deposition of PEEK. This heat input depends not only on the printing temperatures but also on nozzle path. Since the nozzle is the main source of heat in FFF, different nozzle paths correspond to different temperature profiles and different cooling rates. This can be especially important in PEEK 3D printing since cooldown rates have significant effects in PEEK’s crystalline contents [49] which, in turn, are related to 3D printed PEEK’s mechanical behaviour [33, 34]. On top of this, the experimental results of this work also show that this heat input can be related to deposition stability and

consequently to the presence and volume of void defects in printed samples.

Considering this relation, the deposition sequence in a printed layer dictates how the temperature from the nozzle and the deposited material is distributed to the deposition zone. This effect was observed in the previous section for the inner laps of the concentric pattern samples where the nozzle spent more time in a relatively small area of the layer resulting in higher temperature deposition zones that hindered deposition stability. According to this, these patterns could benefit from different deposition sequences for the concentric laps where heat from the nozzle could be more evenly distributed throughout the layer. To test this, G-code files of the concentric samples 01C and 01S were edited to print the concentric laps in two different sequences, one alternating between inner and outer laps (“A”) and one where the layers are built alternating between inside-out and outside-in (“I”).

With these samples, the conditions created by the extrusion calibration described in the beginning of this work can change completely. Furthermore, the retraction setting in the modified printing files was kept for the outermost lap of the samples which might be the incorrect approach given the modified deposition sequence. Perhaps for these reasons, the modified printing files for samples 01S-A and 01S-I resulted in unstable deposition (Fig. 12a and b) and could not be tested without changing print conditions significantly. Despite this, good quality deposition was obtained with 01C-A and 01C-I samples (Fig. 12c and d) which were submitted to density measurements and compression testing. The results for these tests are provided in Table 4.

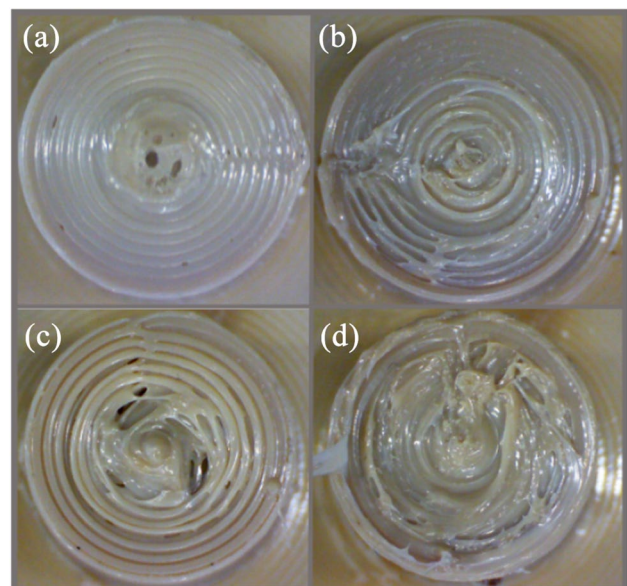


Fig. 12 Layer deposition for samples 01C-A (a), 01C-I (b), 01S-A (c) and 01S-I (d) with modified deposition sequence

Fig. 13 Schematic illustration of nozzle heat distribution for deposition sequences of samples 01C (a), 01C-A (b) and 01C-I (c)

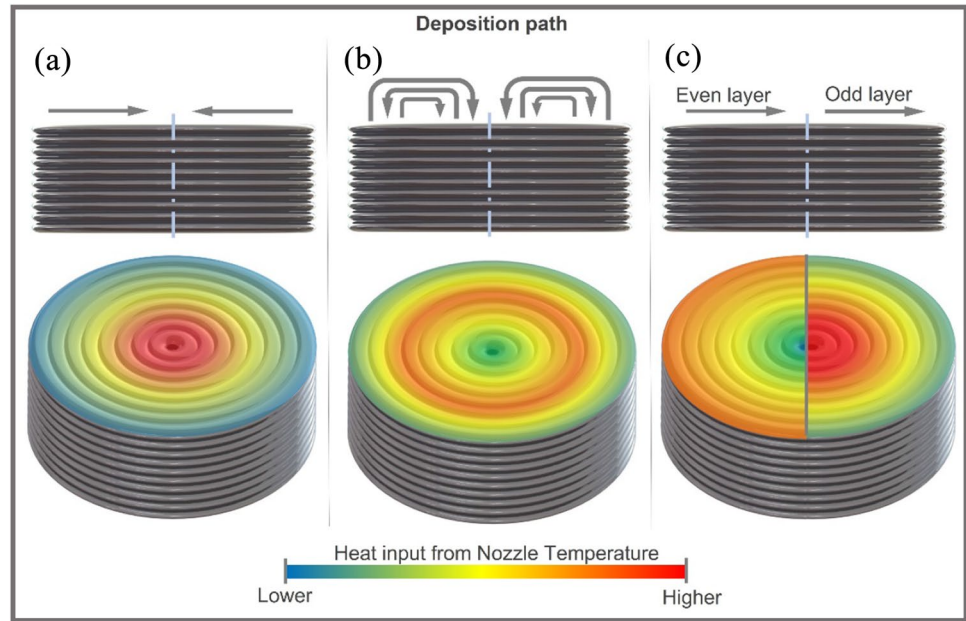


Table 4 Density and compression test results for different deposition patterns

	Density (g/cm ³)	Porosity (%)	Modulus, E (GPa)	Yield strength, $\sigma_{0,2\%}$ (MPa)	Modulus, E_{bulk} (GPa)	Yield strength, $\sigma_{0,2\%bulk}$ (MPa)
01C	1.255 ± 0.010	2.68 ± 0.22	3.12 ± 0.06	94.4 ± 1.7	3.20 ± 0.06	96.6 ± 1.7
01C-A	1.280 ± 0.002	1.53 ± 0.14	3.4 ± 0.04	95.2 ± 1.2	3.45 ± 0.04	97.0 ± 1.2
01C-I	1.203 ± 0.024	7.47 ± 0.30	2.78 ± 0.05	75.0 ± 2.4	3.00 ± 0.05	81.0 ± 2.4

The expected nozzle heat distribution created by the different deposition sequences can be described through the radial nozzle path as schematically represented in Fig. 13. In samples 01C, since the build sequence remains inside-out, the smaller length inner laps accumulate heat from the nozzle that can be dissipated while the longer outer layers are being printed. In this configuration, since lines are deposited sequentially next to each other, cooldown rates are mostly dictated by line length and layer size and geometry. Conversely, for samples 01C-I where the sequence is alternated between layers, the heat input from the nozzle is accentuated in the region where the current layer ends and the next layer begins resulting in higher temperature regions that alternate between the outer and inner regions of the specimen. Lastly, with samples 01C-A the alternating the lap sequence inside the layer allows both inner and outer regions to cooldown while the next lap is printing. This distributes the heat from the nozzle more evenly through the layer while maintaining a relatively high temperature on the deposition region.

The results from the density measurements and compression tests presented in Table 4 show that deposition sequence can have a significant impact in the overall quality of PEEK 3D printed samples. Samples 01C-I display a much higher

estimated void volume when compared to 01C thus resulting in significantly lower values for both compressive yield strength and modulus. In this configuration, the temperature build-ups described in the previous section are accentuated and inner region of the print remains in the molten state before the next layer begins inside-out. This causes the nozzle to stir the material from the deposition region in the melt state thus creating large-scale void defects that could be the reason for the higher estimated void volume observed with these samples. Considering that this deposition sequence increases heat input in both the inner and outer regions of concentric deposition, it might be more adequate for prints with larger layers where sufficient cooldown is allowed.

Contrarily, the deposition sequence used in samples 01C-A yielded positive results. The estimated void volume was reduced to 1.53% while both yield strength and modulus were increased to 95.2 MPa and 3.4 GPa respectively, in relation to samples 01C. These results are comparable to those obtained with the interlayer offset deposition “S”. These improvements can be attributed to the cooling of the inner laps while the outer lap is being printed which seems to improve deposition quality and reduce the presence of void defects in the samples. Interestingly, alternating

deposition between inner and outer concentric laps has the potential to adjust the heat input from the nozzle to line length. Using this strategy, the longer outside laps allow the core of the print to cooldown while the smaller inner laps prevent excessive cooling of the outer laps before its adjacent line is deposited. This is well suited to smaller concentric layers where the inner laps tend to build up temperature from the nozzle.

Although the relation between printing temperatures and the interfacial bonding and crystallinity of printed PEEK has been previously studied [33, 34], the idea that deposition sequence can produce similar effects has yet to be addressed. The deposition sequence's influence in the distribution of heat from the nozzle has a direct effect on the cooldown rates of the deposited material. Slower cooldown rates are related to higher crystallinity PEEK [49] which displays higher strength and fracture toughness [50]. Also, the temperature of the deposition zone is related to the molecular bonding of the deposited material [30] meaning that deposition sequence can have an effect on the interfacial bonding strength of 3D printed PEEK.

To address these effects, the results from the compression tests were used to estimate the properties of equivalent bulk printed samples where the cross-section area is calculated based on porosity estimates. The estimated yield strength ($\sigma_{0.2\%bulk}$) and modulus (E_{bulk}) are shown in Table 4 which, together with crystallinity measurements from DSC tests (Table 5), can provide some additional insights to the effects of deposition sequence on both crystallinity and interfacial bonding.

Considering bulk PEEK prints, some significant differences can still be seen in both yield strength and stiffness. Although samples 01C and 01C-A seem equivalent in strength, the alternating deposition still results in higher stiffness. The estimates obtained for bulk samples seem to suggest that, apart from the effects on deposition stability and consequent porosity, deposition sequence can influence the stiffness of printed PEEK. This can be explained by the crystallinity percentage obtained from DSC measurements where the modified deposition sequences showed higher crystalline contents than 01C samples. Both samples 01C-A and 01C-I can have a higher heat input from the nozzle at mid radius from where the DSC samples were taken which can be the reason for these increases in crystallinity.

The results from these experiments suggest that deposition sequence also has significant effects on the density and

mechanical behaviour of 3D printed PEEK samples. This has yet to be tested with the interlayer line offset deposition "S" where the lower void volumes of the samples could be reduced even further. Adjusting both deposition pattern and sequence appears to be an effective approach to increase the strength and modulus of PEEK prints. However, adequate deposition also depends on sample size and geometry meaning that adjustments to 3D printing parameters for low porosity PEEK prints must consider all three factors addressed in this work, printing temperatures, deposition pattern and deposition sequence. Considering this, the results from this work suggest that printing parametrization for high-quality PEEK prints should consider the model's geometry to determine adequate deposition strategies and corresponding printing temperatures which can then be adjusted to obtain denser high-performance PEEK 3D prints as illustrated in Fig. 14.

4 Conclusions

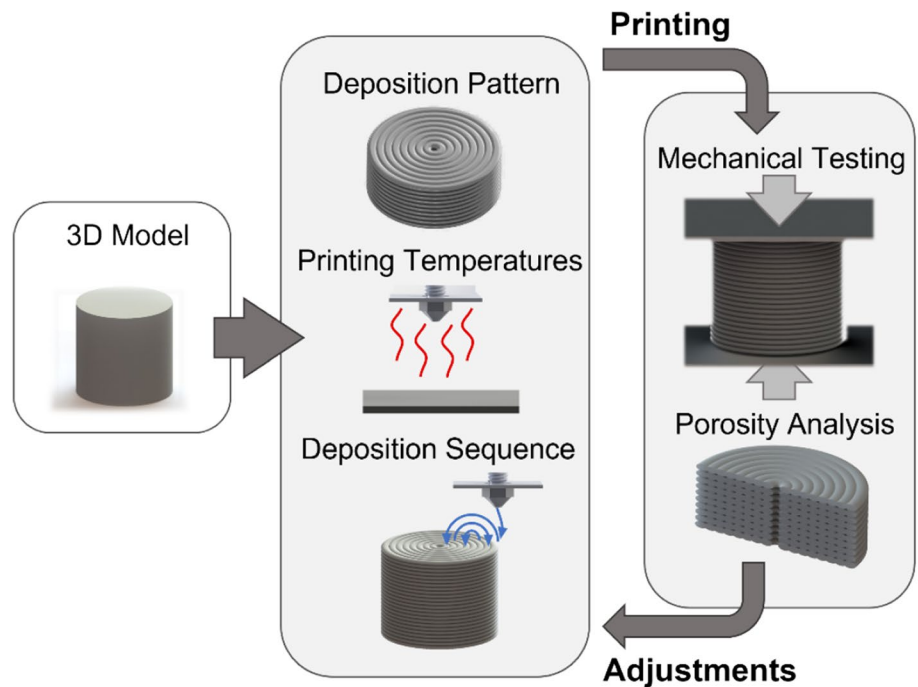
The effects of 3D printing temperatures, deposition pattern and deposition sequence were studied through the density and compressive behaviour of PEEK 3D printed samples. Compression test specimens were printed with different deposition patterns and were tested with different NT and ZHT to investigate the effects of process heat input in the deposition stability for different patterns. These effects were observed in the experimental results where the void contents were related to the samples' compressive properties. In addition, different deposition sequences were tested for the concentric pattern to observe the relation between different nozzle heat distributions and deposition quality.

The results from this work show that printing temperatures and deposition strategies have significant effects in PEEK prints. For the tested cylindrical specimens, the concentric pattern is more adequate since the estimated void volume of 2.68% is about 45% lower than that obtained with the rectilinear deposition. The estimated void volume of the samples is reflected on its compressive properties where the concentric-based deposition resulted in higher yield strength and modulus than the rectilinear samples. Among the concentric patterns tested, the interlayer line offset deposition presented the best results of all experiments with an estimated void volume of 0.72%, yield strength of 100.3 GPa and modulus of 3.58 GPa.

Table 5 DSC results for thermal properties and crystallinity percentage of concentric samples printed with different deposition sequence

	T_g (°C)	T_m (°C)	ΔH_m (J.g ⁻¹)	T_{hc} (°C)	ΔH_{hc}	X_c (%)
01C	148.1 ± 2.2	345.4 ± 0.4	37.58 ± 2.87	296.8 ± 0.1	46.14 ± 0.79	28.9 ± 2.2
01C-A	149.8 ± 3.5	343.2 ± 0.9	42.95 ± 1.66	297.0 ± 0.3	48.62 ± 0.89	33.0 ± 1.3
01C-I	147.9 ± 4.7	344.6 ± 0.6	38.71 ± 2.22	296.6 ± 0.2	47.31 ± 2.24	29.8 ± 1.7

Fig. 14 Schematic representation of the parameter adjustment procedure for high-performance PEEK 3D printing



Concerning the different temperature settings, the results showed that the effect of these temperatures on deposition stability vary according to deposition pattern. Increases in ZHT resulted in increases in stiffness but further increases of process temperatures also resulted in higher void volume and lower compressive strength and stiffness for all patterns. However, with the interlayer line offset deposition “S”, increases in printing temperatures seem to improve its gap filling effect which resulted in lower void volume and higher compressive modulus. Similarly, deposition stability was also improved by adopting the alternating deposition sequence in sample 01C-A and resulted in a reduction of about 42% in void volume compared to the deposition of samples 01C.

Since 3D printed PEEK’s potential lies with high-performance applications that have requirements for strength and stiffness, understanding the relations between process parameters and the mechanical behaviour of 3D printed PEEK samples is an important step for its use in applications like patient-specific load-bearing orthopaedic implants. This work shows that both printing temperatures and deposition strategy must be adjusted together according to the print’s geometry to minimize the void contents of the prints and consequently maximize the strength and stiffness of PEEK 3D printed components. Although additional experimental work is required to study these effects, this work shows that printing temperatures affect deposition stability and bonding quality differently depending on the deposition pattern which in turn is also related to the mechanical behaviour of 3D printed PEEK. Considering this, future research is

required to address how the heat input created by both printing temperatures and deposition strategy is related to deposition quality and to the presence of void defects in 3D printed PEEK components.

Acknowledgements The authors acknowledge Fundação para a Ciência e a Tecnologia (FCT-MCTES) for its financial support through the PhD scholarship UI/BD/151082/2021, through the UNIDEMI projects UIDB/00667/2020 and UIDP/00667/2020 and through IDMEC under LAETA, project UIDB/50022/2020.

Funding Open access funding provided by FCTIFCCN (b-on).

Declarations

Conflict of interest On behalf of all authors, the corresponding author states that there is no conflict of interest.

Open Access This article is licensed under a Creative Commons Attribution 4.0 International License, which permits use, sharing, adaptation, distribution and reproduction in any medium or format, as long as you give appropriate credit to the original author(s) and the source, provide a link to the Creative Commons licence, and indicate if changes were made. The images or other third party material in this article are included in the article’s Creative Commons licence, unless indicated otherwise in a credit line to the material. If material is not included in the article’s Creative Commons licence and your intended use is not permitted by statutory regulation or exceeds the permitted use, you will need to obtain permission directly from the copyright holder. To view a copy of this licence, visit <http://creativecommons.org/licenses/by/4.0/>.

References

1. Gibson I, Rosen D, Stucker B, Khorasani M (2021) Additive manufacturing technologies, 3rd edn. Springer International Publishing. <https://doi.org/10.1007/978-3-030-56127-7>
2. Sachs E, Cima M, Cornie J, Brancazio D, Brecht J, Curodeau A et al (1993) Three-dimensional printing: the physics and implications of additive manufacturing. *CIRP Ann Manuf Technol* 42:257–260. [https://doi.org/10.1016/S0007-8506\(07\)62438-X](https://doi.org/10.1016/S0007-8506(07)62438-X)
3. Thompson MK, Moroni G, Vaneker T, Fadel G, Campbell RI, Gibson I et al (2016) Design for additive manufacturing: trends, opportunities, considerations, and constraints. *CIRP Ann Manuf Technol* 65:737–760. <https://doi.org/10.1016/j.cirp.2016.05.004>
4. Ali MA, Rajabi M, Sudhir SS (2020) Additive manufacturing potential for medical devices and technology. *Curr Opin Chem Eng* 28:127–133. <https://doi.org/10.1016/j.coche.2020.05.001>
5. Haryńska A, Carayon I, Kosmela P, Szeliski K, Łapiński M, Pokrywczyńska M et al (2020) A comprehensive evaluation of flexible FDM/FFF 3D printing filament as a potential material in medical application. *Eur Polym J* 138:109958. <https://doi.org/10.1016/j.eurpolymj.2020.109958>
6. Garcia J, Yang ZL, Mongrain R, Leask RL, Lachapelle K (2018) 3D printing materials and their use in medical education: a review of current technology and trends for the future. *BMJ Simul Technol Enhanc Learn* 4:27–40. <https://doi.org/10.1136/bmjstel-2017-000234>
7. Kalita SJ, Bose S, Hosick HL, Bandyopadhyay A (2003) Development of controlled porosity polymer-ceramic composite scaffolds via fused deposition modeling. *Mater Sci Eng C* 23:611–620. [https://doi.org/10.1016/S0928-4931\(03\)00052-3](https://doi.org/10.1016/S0928-4931(03)00052-3)
8. Green S, Schlegel J (2001) A polyaryletherketone biomaterial for use in medical implant applications. In: *Polym Med Ind Proc a Conf Held Brussels*, pp 1–7.
9. Kurtz SM (2012) PEEK biomaterials handbook, 1st edn. Elsevier
10. Kurtz SM, Devine JN (2007) PEEK biomaterials in trauma, orthopedic, and spinal implants. *Biomaterials* 28:4845–4869. <https://doi.org/10.1016/j.biomaterials.2007.07.013>
11. Anandkumar R, Babu SR (2019) FDM filaments with unique segmentation since evolution: a critical review. *Prog Addit Manuf* 4:185–193. <https://doi.org/10.1007/s40964-018-0069-8>
12. da Silva LRR, Sales WF, dos Campos FAR, de Sousa JAG, Davis R, Singh A et al (2021) A comprehensive review on additive manufacturing of medical devices, vol 6. Springer International Publishing. <https://doi.org/10.1007/s40964-021-00188-0>
13. Wazeer A, Das A, Sinha A, Inaba K, Ziyi S, Karmakar A (2022) Additive manufacturing in biomedical field: a critical review on fabrication method, materials used, applications, challenges, and future prospects. Springer International Publishing. <https://doi.org/10.1007/s40964-022-00362-y>
14. Weinans H, Huijskes R, Grootenboer HJ (1992) Effects of material properties of femoral hip components on bone remodeling. *J Orthop Res* 10:845–853. <https://doi.org/10.1002/jor.1100100614>
15. Singh S, Singh G, Prakash C, Ramakrishna S (2020) Current status and future directions of fused filament fabrication. *J Manuf Process* 55:288–306. <https://doi.org/10.1016/j.jmapro.2020.04.049>
16. Ahn SH, Montero M, Odell D, Roundy S, Wright PK (2002) Anisotropic material properties of fused deposition modeling ABS. *Rapid Prototyp J* 8:248–257. <https://doi.org/10.1108/13552540210441166>
17. Es-Said OS, Foyos J, Noorani R, Mendelson M, Marloth R, Pregarer BA (2000) Effect of layer orientation on mechanical properties of rapid prototyped samples. *Mater Manuf Process* 15:107–122. <https://doi.org/10.1080/10426910008912976>
18. Masood SH, Mau K, Song WQ (2010) Tensile properties of processed FDM polycarbonate material. *Mater Sci Forum* 654–656:2556–2559. <https://doi.org/10.4028/www.scientific.net/MSF.654-656.2556>
19. Durgun I, Ertan R (2014) Experimental investigation of FDM process for improvement of mechanical properties and production cost. *Rapid Prototyp J* 20:228–235. <https://doi.org/10.1108/RPJ-10-2012-0091>
20. Wu W, Geng P, Li G, Zhao D, Zhang H, Zhao J (2015) Influence of layer thickness and raster angle on the mechanical properties of 3D-printed PEEK and a comparative mechanical study between PEEK and ABS. *Materials (Basel)* 8:5834–5846. <https://doi.org/10.3390/ma8095271>
21. Pu J, McIlroy C, Jones A, Ashcroft I (2021) Understanding mechanical properties in fused filament fabrication of polyether ether ketone. *Addit Manuf* 37:101673. <https://doi.org/10.1016/j.addma.2020.101673>
22. Rinaldi M, Ghidini T, Cecchini F, Brandao A, Nanni F (2018) Additive layer manufacturing of poly (ether ether ketone) via FDM. *Compos Part B Eng* 145:162–172. <https://doi.org/10.1016/j.compositesb.2018.03.029>
23. Avanzini A, Petrogalli C, Battini D, Donzella G (2018) Influence of micro-notches on the fatigue strength and crack propagation of unfilled and short carbon fiber reinforced PEEK. *Mater Des* 139:447–456. <https://doi.org/10.1016/j.matdes.2017.11.039>
24. Colmer T, Daniewicz SR, Newman JC, Moser R (2017) Measuring fatigue crack growth and closure in Polyether Ether Ketone (PEEK). *Int J Fatigue* 95:243–251. <https://doi.org/10.1016/j.ijfatigue.2016.10.025>
25. Wang P, Zou B, Xiao H, Ding S, Huang C (2019) Effects of printing parameters of fused deposition modeling on mechanical properties, surface quality, and microstructure of PEEK. *J Mater Process Technol* 271:62–74. <https://doi.org/10.1016/j.jmatprotec.2019.03.016>
26. Rodriguez J (1999) Maximizing the strength of fused-deposition ABS plastic parts. In: *10th Solid Free*, pp 335–42
27. Rodriguez JF, Thomas JP, Renaud JE (2000) Characterization of the mesostructure of fused-deposition acrylonitrile-butadiene-styrene materials. *Rapid Prototyp J* 6:175–185. <https://doi.org/10.1108/13552540010337056>
28. Rendas P, Figueiredo L, Geraldo M, Vidal C, Soares BA (2023) Improvement of tensile and flexural properties of 3D printed PEEK through the increase of interfacial adhesion. *J Manuf Process* 93:260–274. <https://doi.org/10.1016/j.jmapro.2023.03.024>
29. Rendas P, Figueiredo L, Machado C, Mourão A, Vidal C, Soares B (2022) Mechanical performance and bioactivation of 3D-printed PEEK for high-performance implant manufacture: a review. *Prog Biomater*. <https://doi.org/10.1007/s40204-022-00214-6>
30. Fitzharris ER, Watt I, Rosen DW, Shofner ML (2018) Interlayer bonding improvement of material extrusion parts with polyphenylene sulfide using the Taguchi method. *Addit Manuf* 24:287–297. <https://doi.org/10.1016/j.addma.2018.10.003>
31. Basgul C, Yu T, MacDonald DW, Siskey R, Marcolongo M, Kurtz SM (2020) Does annealing improve the interlayer adhesion and structural integrity of FFF 3D printed PEEK lumbar spinal cages? *J Mech Behav Biomed Mater* 102:103455. <https://doi.org/10.1016/j.jmbbm.2019.103455>
32. Regis M, Bellare A, Pascolini T, Bracco P (2017) Characterization of thermally annealed PEEK and CFR-PEEK composites: structure-properties relationships. *Polym Degrad Stab* 136:121–130. <https://doi.org/10.1016/j.polydegradstab.2016.12.005>
33. Qu H, Zhang W, Li Z, Hou L, Li G, Fuh JY et al (2022) Influence of thermal processing conditions on mechanical and material properties of 3D printed thin-structures using PEEK material. *Int J Precis Eng Manuf* 23:689–699. <https://doi.org/10.1007/s12541-022-00650-1>

34. Lee A, Wynn M, Quigley L, Salviato M, Zobeiry N (2022) Effect of temperature history during additive manufacturing on crystalline morphology of PEEK. *Adv Ind Manuf Eng* 4:100085. <https://doi.org/10.1016/j.aime.2022.100085>
35. Wang Y, Müller WD, Rumjahn A, Schmidt F, Schwitalla AD (2021) Mechanical properties of fused filament fabricated PEEK for biomedical applications depending on additive manufacturing parameters. *J Mech Behav Biomed Mater* 115:104250. <https://doi.org/10.1016/j.jmbbm.2020.104250>
36. Apium PEEK 450 Natural Datasheet. n.d.
37. Park SJ, Lee JE, Park J, Lee NK, Son Y, Park SH (2021) High-temperature 3D printing of polyetheretherketone products: perspective on industrial manufacturing applications of super engineering plastics. *Mater Des* 211:110163. <https://doi.org/10.1016/j.matdes.2021.110163>
38. Hu B, Duan X, Xing Z, Xu Z, Du C, Zhou H et al (2019) Improved design of fused deposition modeling equipment for 3D printing of high-performance PEEK parts. *Mech Mater* 137:103139. <https://doi.org/10.1016/j.mechmat.2019.103139>
39. Crockett RS, Calvert PD (1996) The liquid-to-solid transition in stereodeposition techniques. In: *Process 1996 Int Solid Free Fabr Symp*, pp 257–64
40. Venkataraman N, Rangarajan S, Matthewson MJ, Safari A, Danforth SC, Yardimci A (1999) Mechanical and rheological properties of feedstock material for fused deposition of ceramics and metals (FDC and FDMet) and their relationship to process performance. *Solid Free Fabr Proc* 1999:351–359
41. Yardimci M a, Hattori T, Guceri SI, Danforth SC (1997) Thermal analysis of Fused Deposition. In: *Solid Free Fabr Proceedings, 1997*:689–98
42. Gupta H, Salovey R (1990) Thermal behavior of transparent poly(etheretherketone)(PEEK) film. *Polym Eng Sci* 30:453–458. <https://doi.org/10.1002/pen.760300805>
43. Bonmatin M, Chabert F, Bernhart G, Djilali T (2021) Rheological and crystallization behaviors of low processing temperature poly(aryl ether ketone). *J Appl Polym Sci*. <https://doi.org/10.1002/app.51402>
44. Blundell DJ, Osborn BN (1983) The morphology of poly(aryl-ether-ether-ketone). *Polymer (Guildf)* 24:953–958. [https://doi.org/10.1016/0032-3861\(83\)90144-1](https://doi.org/10.1016/0032-3861(83)90144-1)
45. Agarwala MK, Jamalabad VR, Langrana NA, Safari A, Whalen PJ, Danforth SC (1996) Structural quality of parts processed by fused deposition. *Rapid Prototyp J* 2:4–19
46. Spece H, Yu T, Law AW, Marcolongo M, Kurtz SM (2020) 3D printed porous PEEK created via fused filament fabrication for osteoconductive orthopaedic surfaces. *J Mech Behav Biomed Mater*. <https://doi.org/10.1016/j.jmbbm.2020.103850>
47. Vaezi M, Yang S (2015) Extrusion-based additive manufacturing of PEEK for biomedical applications. *Virtual Phys Prototyp* 10:123–135. <https://doi.org/10.1080/17452759.2015.1097053>
48. Han X, Yang D, Yang C, Spintzyk S, Scheideler L, Li P et al (2019) Carbon fiber reinforced PEEK composites based on 3D-printing technology for orthopedic and dental applications. *J Clin Med* 8:240. <https://doi.org/10.3390/jcm8020240>
49. Naffakh M, Gómez MA, Ellis G, Marco C (2003) Thermal properties, structure and morphology of PEEK/thermotropic liquid crystalline polymer blends. *Polym Int* 52:1876–1886. <https://doi.org/10.1002/pi.1276>
50. Talbott MF, Springer GS, Berglund LA (1987) The effects of crystallinity on the mechanical properties of PEEK polymer and graphite fiber reinforced PEEK. *J Compos Mater* 21:1056–1081. <https://doi.org/10.1177/002199838702101104>

Publisher's Note Springer Nature remains neutral with regard to jurisdictional claims in published maps and institutional affiliations.